Progress In Electromagnetics Research, PIER 61, 111–131, 2006

LOCALIZATION OF THE INVESTIGATION DOMAIN IN INVERSE PROFILING OF BURIED 2-D DIELECTRIC PIPELINES WITH CIRCULAR CROSS SECTION USING ELECTROMAGNETIC SCATTERED DATA

V. Thomas, J. Yohannan, A. Lonappan, G. Bindu and K. T. Mathew

Microwave Tomography and Materials Research Laboratory
Department of Electronics
Cochin University of Science and Technology
Kochi-682 022, India

Abstract—Electromagnetic inverse scattering problems are computation intensive, ill-posed and highly non-linear. When the scatterer lies in an inaccessible domain, the ill-posedness is even more severe as only aspect limited data is available. Typical algorithms employed for solving this inverse scattering problem involve a large scale non-linear optimization that generates values for all pixels in the investigation domain including those that might not contain any useful information about the object. This communication is concerned with the localization in the investigation domain prior to inverse profiling of buried 2-D dielectric pipelines having circular cross section. A custom defined degree of symmetry is computed for each transmitter position, which is a measure of the symmetry of the measured (synthetic) scattered field vector. The degree of symmetry vector computed for a scatterer is found to exhibit unique features for the geometric and electric properties of the dielectric pipeline. A probabilistic neural network is trained with the degree of symmetry vectors computed for different object configurations. It classifies the test degree of symmetry vector of the unknown scatterer presented to it into one of the classes that indicate the localized region in the investigation domain in which the pipeline is located. The Distorted Born Iterative procedure is employed for imaging the pipeline that has been localized. The reduction in the investigation domain reduces the degrees of freedom of the inverse scattering problem and the results are found to be much superior to those when the entire investigation domain is employed.

1. INTRODUCTION

The development of imaging techniques for investigation of physically inaccessible objects is of much importance in areas such as oil exploration, seismic imaging, non destructive evaluation, buried object detection etc. In most of these cases, reliable information about the physical properties of the inaccessible target is desired in addition to detection of the target. All these problems may be classified as electromagnetic inverse problems when the characterization of the unknown target is computed by considering electromagnetic illumination and employing the values of the scattered electromagnetic field. This inverse scattering problem is non linear due to multiple scattering and also ill posed, which is very severe due to the availability of aspect limited data only [1].

Many algorithms have been designed to tackle this class of inverse scattering problems. For the detection of buried targets and landmines, a simple model has been proposed by using the Ground penetrating radar (GPR) technique, without accounting for the air-earth interface [2, 3]. To build up more accurate models, a half space problem must be considered to represent the air-earth interface. Several methods that include the modified gradient approach [4, 5], Born iteration and constrained optimization [6], and Distorted Born Iterative method [7] and high-order extended Born approximations [8] have been investigated for the buried object problem. All these methods solve a large-scale, non-linear optimization problem by generating values for every pixel covering the investigation domain, including those which might not contain any useful information about the objects. The investigation domain has to be chosen sufficiently large to include all possible target locations. Due to the non linearity of the inverse scattering problem, the solutions are liable to get trapped in local minima. When the investigation domain is large, the number of unknowns of the inverse scattering problem increases and an iterative procedure for solving the inverse problem may fail to reach a convergent solution in addition to increasing the computation time [9]. Neural Networks have been employed to detect 2-D dielectric scatterers when only aspect limited scattered data is measurable, with the a priori knowledge that the scatterer is 2-D homogenous and with a circular cross section [10, 11].

In this communication the a priori knowledge about the cylindrical geometry of the buried 2-D dielectric pipeline, which is possibly located in the inaccessible investigation domain is exploited, with the assumption that the complex permittivity distribution is symmetric with respect to the centre of the cross section. The cross sectional

profiles considered for the cylinder are a homogenous profile and a cross sectional profile of two concentric circles, which are the practical cases for a buried pipeline. The investigation domain is illuminated with TM polarized harmonic excited electromagnetic radiation. Scattered data can be measured only in a limited angle, as the imaging domain is inaccessible. The following situation is investigated: the pipeline is buried in wet soil in which case a half space problem is considered to account for the air-soil interface. A localization of the dielectric pipeline in the investigation domain is done prior to the cross sectional profiling, which will reduce the number of unknowns. For each transmitter view, a custom defined scalar parameter called degree of symmetry, a function of the symmetry of the scattered field vector measured by the receivers, is computed. Thus for a particular object configuration, there will be an associated degree of symmetry vector which comprises of the scalar values computed for each transmitter view. A Probabilistic Neural Network (PNN) is then trained with the degree of symmetry vectors computed for a training set of object configurations. PNN offers the advantage of rapid training and easy re-trainability. It is also guaranteed to converge to the Bayesian classifier, the optimal classifier, with enough training data [12]. It classifies the degree of symmetry vector of the unknown scatterer presented to it into one of the classes that indicate the localized region in the investigation domain. Thus the degrees of freedom in the inversion for the buried pipeline are reduced, which aids the global convergence of the solution. It also results in a reduction in computation time. The Distorted Born Iterative procedure is employed to image the scatterer that has been localized [7]. The details of the formulation of the problem and numerical simulations and discussions are presented in this paper.

2. FORMULATION OF THE PROBLEM

The geometry of the problem is as shown in Figure 1, where the homogenous half spaces, air and wet soil, are separated by a planar interface.

The investigation domain D is chosen to be a square or rectangle that possibly contains the buried dielectric pipeline. This should be large enough to include all possible locations of the buried pipeline. The axis of the pipeline is oriented in the z direction so that the cross section lies in the x-y plane. Both media and the scatterer are assumed linear, isotropic, non magnetic and penetrable. The transmitters and receivers are mounted at the same height to reduce the number of the Sommerfield-like integral equations [7]. The y-axis passes through the central transmitter. The transmitters are ideal time harmonic electric

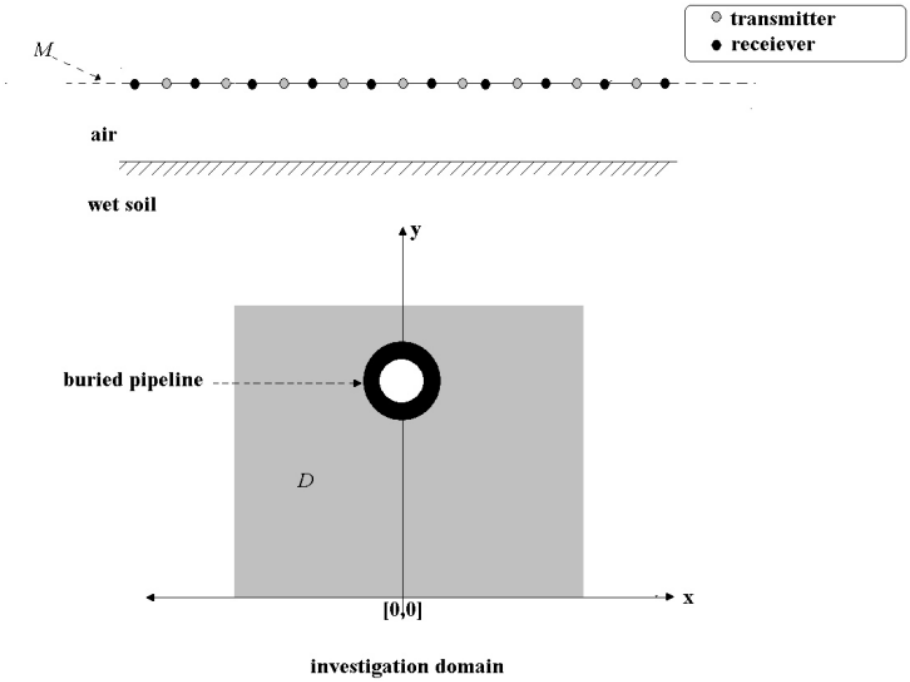

Figure 1. The experimental setup. The central transmitter $\frac{N_r}{2}$ is aligned with the y-axis.

current line sources, set parallel to the z-axis (polarized), and mounted at a height y_s from the origin in the measurement domain M. The receivers are also ideal and the number of receivers is one more than that of the transmitters, as there will be a receiver antenna on either side of a transmitter antenna. The measurement setup is assumed movable in the direction. The scattering problem is scalar, and only the z component of the scattered field is needed. A time convention of $e^{-j\omega t}$ is assumed and suppressed in the scattering integral equations.

The forward problem is formulated employing the domain integral equations, where

$$e^{total}(r) = e^{incident}(r) + \int_D \delta(r')g_{ss}(r,r')e^{total}(r')dr', \quad r \in D \qquad (1)$$

is the state equation and

$$e_{scat}(r) = \int_D \delta(r')g_{as}(r,r')e^{total}(r')dr', \quad r \in M \qquad (2)$$

is the observation equation [7].

In the above equations, $e^{total}(r)$ and $e^{incident}(r)$ are the total and incident fields at the point r and $\delta(r)$ the dielectric contrast given by $\delta(r) = \varepsilon_r(r) - \varepsilon_{background},\ r \in D$ with $\varepsilon_{background}$ being the permittivity of wet soil. Here g_{ss} is the half space Green's function when r and r' are in the half space wet soil and g_{as} the half space Green's function when r is in the half space air and r' in the half space wet soil. The integral equations are discretized with pulse basis functions and point matching method of moments [13]. The discretized state and observation equations for each transmitter view are

$$e_v^{incident} = [I - G_{SS}D(c)]e_v^{total} \tag{3}$$

and

$$e_v^{scat} = G_{AS}D(c)e_v^{total} \tag{4}$$

where e_v^{total}, $e_v^{incident}$ and c are the total electric field vector, the incident field vector and the complex permittivity contrast vector respectively in D, of dimension $N \times 1$, all in lexicographical order, N being the number of pixels in D. G_{SS} and G_{AS} are the matrices of properly integrated Greens functions of dimension $N \times N$ and $N_r \times N$ respectively where N_r is the number of receivers in M. $D(c)$ is the diagonal matrix of dimension $N \times N$ whose entries are the elements of the contrast vector c [14]. Only the scattered field vector e_v^{scat} of dimension $N_r \times 1$ is available for the reconstruction of the complex permittivity contrast in the inverse scattering problem.

3. SOLUTION PROCEDURE

Inverse scattering algorithms in electromagnetics typically involve large scale non linear optimization techniques that generate the complex permittivity values for every point in the investigation domain D, including those that may not contain any useful information about the scatterer. The number of unknowns in the inverse problem will be large when the investigation domain is large, and an iterative procedure for solving the inverse problem may fail to reach a convergent solution in addition to increasing the computation time. However if the object could be localized in D prior to the inverse scattering, the degrees of freedom of the inverse problem may be reduced. In this paper we employ a custom defined degree of symmetry vector for the purpose of localizing the 2-D dielectric scatterer in the investigation domain, under the assumption that the scatterer cross section is circular. We have considered the homogenous cross sectional profile and a cross sectional profile consisting of two concentric circles, which are the

practical cases for the buried pipeline. The degree of symmetry ($D.O.S$), for a transmitter view v is defined as (assuming even number of receivers N_r per view)

$$D.O.S(v) = abs\left(\sum_{k=1}^{N_r/2}\left\|e_v^{scat}(k) - e_v^{scat}(N_r+1-k)\right\|^2\right), \quad v = 1,2,3,\ldots,N_r-1 \tag{5}$$

where *abs* indicates absolute value.

Thus the $D.O.S$ for a transmitter position is a function of the Euclidean distance between the first half and the spatially reflected second half of the measured scattered field vector. The $D.O.S$ value will be equal to zero when the two halves are exactly similar and maximum when they are most dissimilar. The two halves of the exact measured scattered field vector are identical only for case of the central view $\frac{N_r}{2}$ and when the circularly symmetric pipeline cross section lies symmetric with respect to the measurement array with its centre on the y-axis as in Figure 1. The measurement setup is moved in the x direction until the $D.O.S$ for the central transmitter is minimum, which is when the centre of the pipeline cross section coincides with the y-axis. For this purpose a modified degree of symmetry is computed for each transmitter position as follows:

for $v = 1 : \frac{N_r}{2}$,

$$\begin{aligned} e_{vL} &= e_v^{scat}(r),\ r = 1,2,\ldots,v \text{ and} \\ e_{vR} &= e_v^{scat}(r),\ r = 2v, 2v-1, 2v-2, \ldots, v+1 \end{aligned}$$

for $v > \frac{N_r}{2}$,

$$\begin{aligned} e_{vL} &= e_v^{scat}(r),\ r = 2v-N_r+1,\ldots,v, \\ e_{vR} &= e_v^{scat}(r),\ r = N_r, N_r-1, N_r-2, \ldots, v+1 \end{aligned}$$

$$D.O.S_{\text{mod}}(v) = \frac{1}{(size(e_{vL}))^2} abs\left(sum(e_{vL} - e_{vR})^2\right) \tag{6}$$

Thus the lengths of the first half vector e_{vL} and the spatially reflected second half vector e_{vR} are equal for a given transmitter view v. In equation (5), the degree of symmetry for any given transmitter view v is computed with all the measured scattered values employed for the calculation, whereas in equation (6), the transmitter v is always at the centre of the measurement points employed for computing the modified degree of symmetry. If the buried 2-D cylindrical pipeline is located under a transmitter offset from the central transmitter as

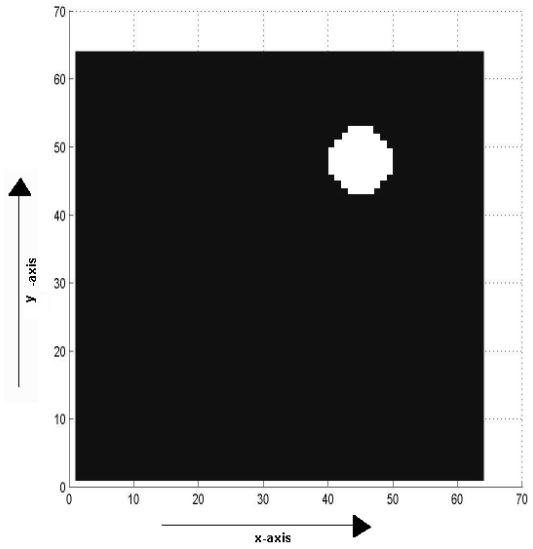

Figure 2a. A 2-D dielectric pipeline with circular cross section is located with its center displaced to the right of the center of the investigation domain.

shown in Figure 2a, the $D.O.S_{\text{mod}}$ value will be equal to zero for that view as shown in Figure 2b. The measurement setup is now moved in the x direction such that the minimum value of $D.O.S_{\text{mod}}$ now coincides with the central transmitter $\frac{N_r}{2}$, which is when the centre of the pipeline cross section coincides with the y-axis as in Figure 1. The new $D.O.S_{\text{mod}}$ vector is plotted in Figure 2c. where the minimum value is for the central transmitter. The scalar $D.O.S$ values are then computed for each transmitter position, which together constitutes a $D.O.S$ vector. In this case, $D.O.S$ vector will be symmetric with respect to its centre, where it has its minimum value. However when the transmitter view is changed to either side of the central view, the scattered field vector e_v^{scat} will not be symmetric with respect to its centre as the receiver array is not symmetric with respect to the transmitter location. Therefore the $D.O.S$ will increase either side of the central view. There will be two views symmetrically located on either side of the central view where e_v^{scat} is most asymmetric and hence the $D.O.S$ is maximum.

The measured scattered field vector is dependent on the distance of the receivers from the scatterer via the Greens function G_{AS} and the total field inside the object e_v^{total} which is a function of the object

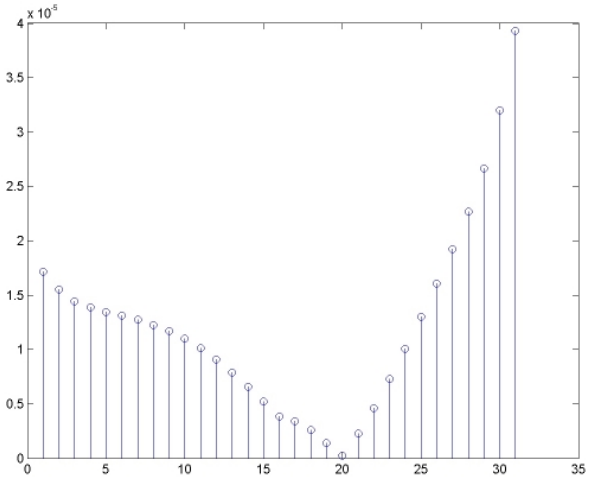

Figure 2b. The modified degree of symmetry $D.O.S_{\text{mod}}$ is plotted for the pipeline in Figure 2a. For the simulation 31 transmitters have been employed. The plot shows that the pipeline center is located under the transmitter 20. The measurement setup is to be moved by 4 transmitter spacing to the right so that the minimum of $D.O.S_{\text{mod}}$ is now aligned with the central transmitter 16.

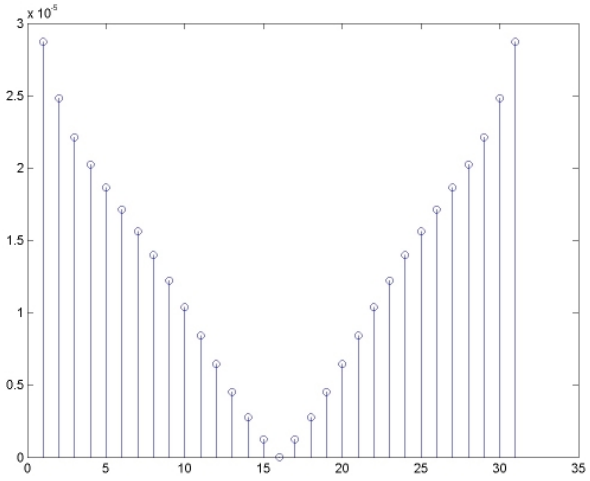

Figure 2c. The modified degree of symmetry $D.O.S_{\text{mod}}$ is plotted from the computed measured scattered field for the new position of the measurement array. The center of the pipeline is now located under the central transmitter, as indicated by the minimum value of $D.O.S_{\text{mod}}$ coinciding with the central transmitter 16.

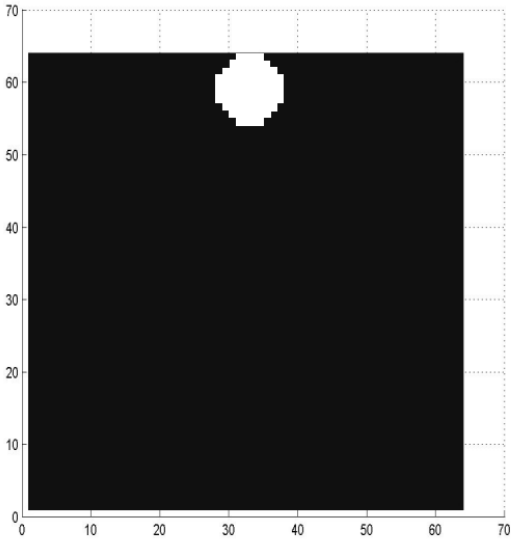

Figure 3a. The pipeline is located at the top of the investigation domain.

contrast c, the incident field $e_v^{incident}$. It is seen that the geometric properties namely the inner and outer radii and the depth at which the scatterer is located in D and the dielectric contrast of the scatterer influence the values and features of the $D.O.S$ vector. For example, consider the pipeline located at the top of the investigation domain, as shown in Figure 3a. The $D.O.S$ for this configuration is plotted in Figure 3b. The same pipeline is shown buried at a greater depth in Figure 3c and the corresponding $D.O.S$ is shown plotted in Figure 3d. In Figure 3e, the pipeline lies buried at the bottom of D and its $D.O.S$ is plotted in Figure 3f. It is observed from Figure 3 that the $D.O.S$ values show a faster increase from the central minimum value to the maximum values on either side, when the object is located at a shallower depth in D.

The features of the $D.O.S$ vector maybe employed to localize the dielectric pipeline in D. For this purpose, a Probabilistic Neural Network (PNN), trained with degree of symmetry vectors for different circularly symmetric scatterers is employed. The PNN was chosen because of its rapid training and easy retraining ability. The PNN provides a general solution for pattern classification problems by following an approach developed in statistics, called Bayesian classifiers [12]. The network paradigm also uses Parzen Estimators, which were

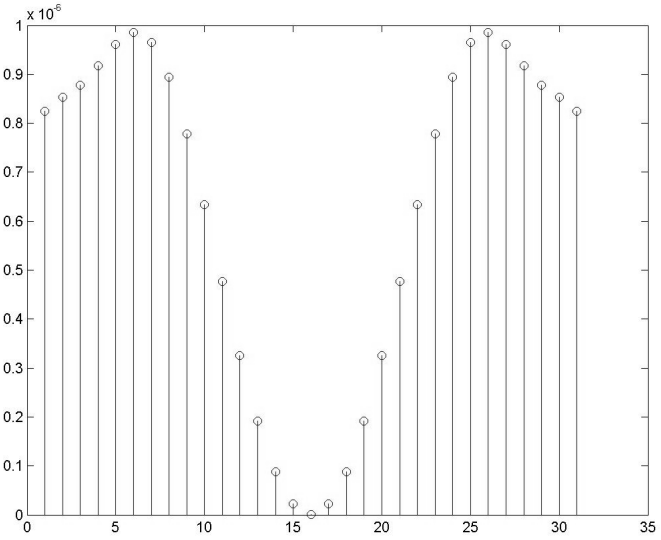

Figure 3b. The $D.O.S$ plotted for the scatterer in Figure 3a.

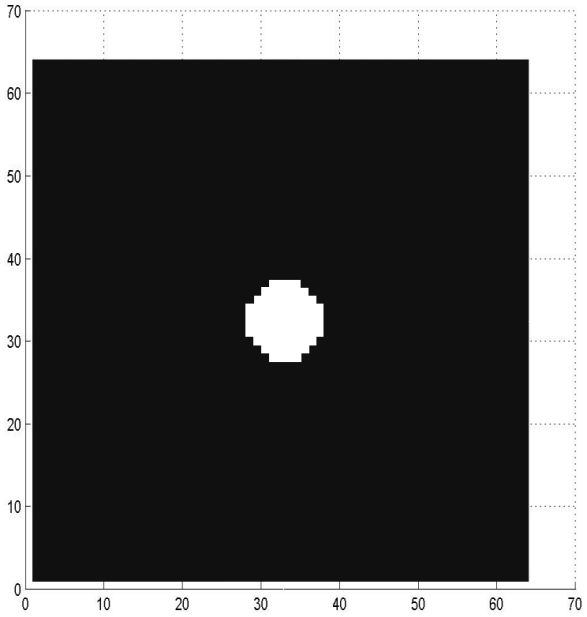

Figure 3c. The same pipeline is located at a greater depth in the investigation domain.

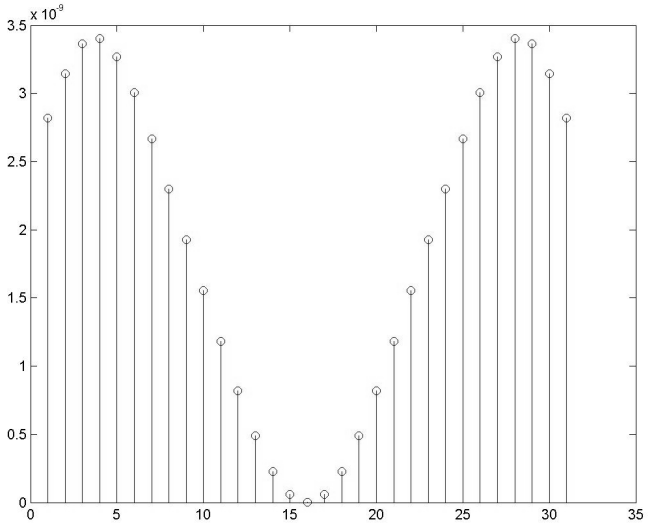

Figure 3d. The $D.O.S$ plotted for the scatterer in Figure 3c. The maxima of the $D.O.S$ are spaced farther apart than in Figure 3b.

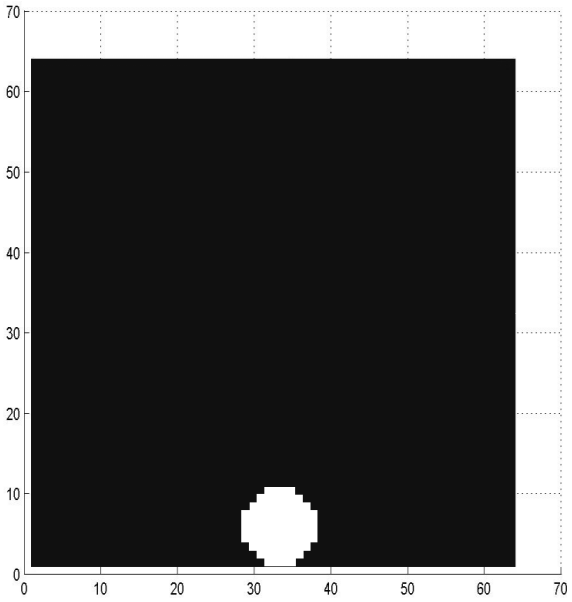

Figure 3e. The pipeline is located at the bottom of the investigation domain.

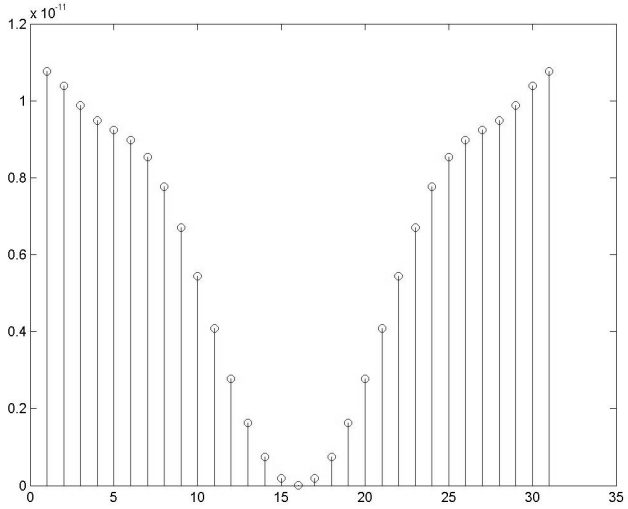

Figure 3f. The $D.O.S$ plotted for the scatterer in Figure 3c. The maxima of the $D.O.S$ are spaced farther apart than in Figure 3d.

developed to construct the probability density functions required by Bayes' theory. The PNN is guaranteed to converge to the Bayesian classifier, which is the optimal classifier, with enough training data. It is also robust in the presence of noise and generalizes well. The architecture of the PNN is shown in Figure 4. The network has four layers: an input distribution layer, a pattern layer, a summation layer and an output decision layer. The distribution layer has as many elements as there are separable parameters needed to describe the objects to be classified. Pattern layer organizes the training set such that each input vector is represented by an individual processing element. The pattern layer weight matrix is set to the transpose of the matrix formed from the input training set, in this case, the training set of $D.O.S$ vectors. The pattern layer transfer function is the Gaussian Probability function centred at each training case. When the standard deviation of the Gaussian function is approaching zero, the PNN approximates a nearest neighbor classifier and when it approaches infinity, the classifier is limited to functions that are linearly separable. Some intermediate value of the standard deviation is usually preferred [15]. An i/p $D.O.S$ vector close to a training $D.O.S$ vector is indicated by a number close to '1' at the corresponding position of the pattern layer o/p vector. The summation layer weights are derived from the target vectors that indicate the localized neighborhood of the dielectric pipeline in D. Each vector has a '1' only in the row associated with

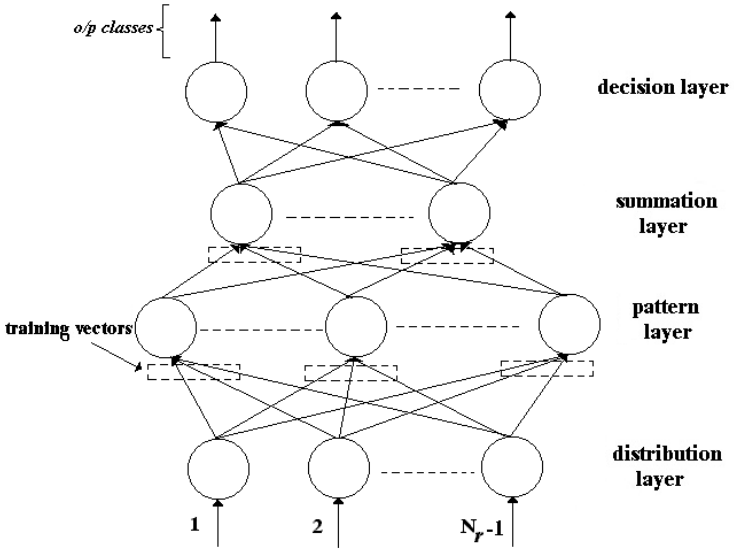

Figure 4. The input test $D.O.S$ vector is classified into one of target output classes that indicate the localized investigation domain.

that particular class of the input $D.O.S$ vector, and 0's elsewhere. Alternately the weights can be adjusted to incorporate the a priori probabilities of each class if it is known. The decision layer employs a competitive transfer function which makes a comparison among the elements of the summation layer output vector. It then outputs a '1' corresponding to the largest element of the summation layer output vector. Thus, the network will classify the input vector into a specific output class that has the maximum probability of being correct.

3.1. Numerical Simulations

The upper region considered here is free space ($\varepsilon_a = 1,\ \delta_a = 0$) and the lower region is wet soil ($\varepsilon_s = 4,\ \sigma_s = 0.005\,\mathrm{s/m}$). The observation equation (3) and state equation (4) are employed for generating synthetic scattered field data in the measurement domain M, for various known circular object profiles buried in wet soil. For the simulation of the experiment, 31 transmitters have been employed in the measurement domain. For each transmitter view, 32 measurements are made at the receiving antenna positions as illustrated in Figure 1. The investigation domain D is chosen to be a square of 2 meters side. The top of the investigation domain is located at a depth of 2.25 meters

from the air-soil interface. The measurement domain is located at a height of 0.75 meters from the air-soil interface. The investigation domain is discretized into $64 \times 64 = 4096$ pixels. The working frequency employed is 100 MHz. Though a higher frequency would have improved the imaging resolution, the depth of penetration of the EM wave will reduce with increasing frequency. The measurement domain is 4 meters long with the transmitters equally spaced on the measurement line and receivers similarly arranged in between the transmitter positions as in Figure 1. The measurement setup is assumed movable in the direction. The cross sectional profiles for the dielectric scatterer considered in this paper are a homogenous profile and a profile consisting of two concentric circles, which are usually the practical cases considered for the dielectric pipeline. The measurement setup is moved in the direction until the $D.O.S$ value for the central transmitter is minimum, which is when the centre of the pipeline cross section lies on the y-axis. The exact scattered fields in the measurement domain are generated with the following parameters of the cylindrical dielectric scatterer:

- For the homogenous profile, the radius is varied in the range 15 centimeters to 45 centimeters. For the concentric circle cross section, the radius of the outer cylinder is varied in the range 30 to sampling intervals to 45 sampling intervals, and the inner radius between 5 sampling intervals and 10 sampling intervals.
- Two ranges of the relative permittivity of the dielectric pipeline are considered. A lossless scatterer is first considered having relative permittivity in the range 2 to 10. A lossy scatterer is also considered with the relative permittivity varied in the range 5 to 10 and conductivity in the range 0.001 to 0.010 S/m. The relative permittivity is varied in steps of 1 and the conductivity is varied in steps of 0.002 S/m.
- The depth at which the cylinder is located in D is varied in steps of 2 sampling intervals.

The Distorted Born Iterative method (DBIM) is employed for the inverse scattering. The $D.O.S$ vectors for the various scatterer configurations are generated from the exact scattered data as per the equation (5). A probabilistic neural network is trained with the training set of $D.O.S$ vectors. The training is virtually instantaneous and involves nothing more than reading in the training vectors and storing them as rows of the pattern layer matrix.

The performance of the algorithm in the presence of noise is also verified. To test the performance of the algorithm in the presence of noise, random white Gaussian noise is added to the synthetic scattered

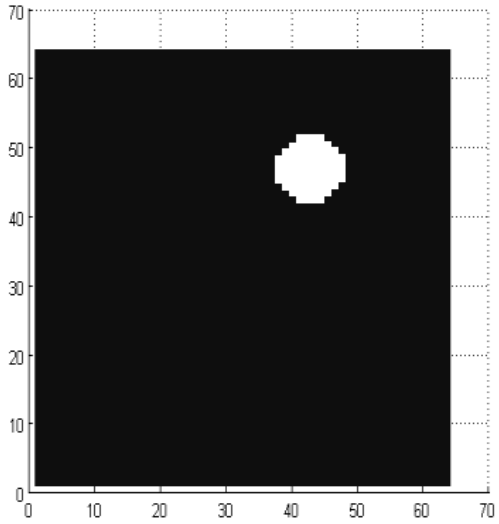

Figure 5a. The actual cross sectional profile of the cylindrical dielectric pipeline ($\varepsilon = 10,\ \sigma = 0.01\,\mathrm{s/m}$.

data. The signal to noise ratio is defined as

$$\frac{S}{N} = 10\log_{10}\frac{\|e_{scat}\|^2}{\|n\|^2}\ \mathrm{dB},$$

where e_{scat} is the exact field data, the norm of the exact field data being obtained after a summation over all the recovers and views, and $\|n\|^2 = 2(N_r - 1)N_r\sigma^2$, where σ is the standard deviation of the random white Gaussian noise.

As an example consider the cylindrical dielectric scatterer ($\varepsilon = 10,\ \sigma = 0.01\,\mathrm{s/m}$) of radius 15 centimeters located at a depth of 0.5 meters from the top of the investigation domain, and the centre of the cross section offset to the right from the centre of the imaging domain by 38 centimeters as shown in Figure 5a. Random white Gaussian noise is added is added to the generated synthetic exact data. The SNR of the scattered field data is 10 dB. The $D.O.S_{\mathrm{mod}}$ values computed from the noisy scattered data are shown plotted in Figure 5b. The plot indicates that the pipeline is located under the transmitter 19. The measurement setup is moved by three transmitters spacing to the right so that the pipeline now lies under the central transmitter 16. The $D.O.S$, computed from the measured scattered field is plotted in Figure 5b. The calculated $D.O.S$ vector is presented to the PNN, which

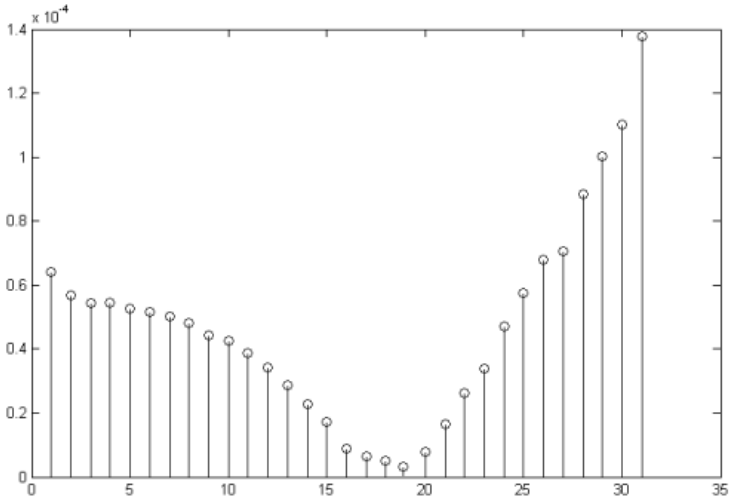

Figure 5b. The $D.O.S_{\text{mod}}$ vector for the scatterer in Figure 5a is plotted above. It indicates that the measurement domain is to be moved to the right in the x-direction by three transmitter spacing so that the $D.O.S$ minimum will be aligned with the central transmitter 16.

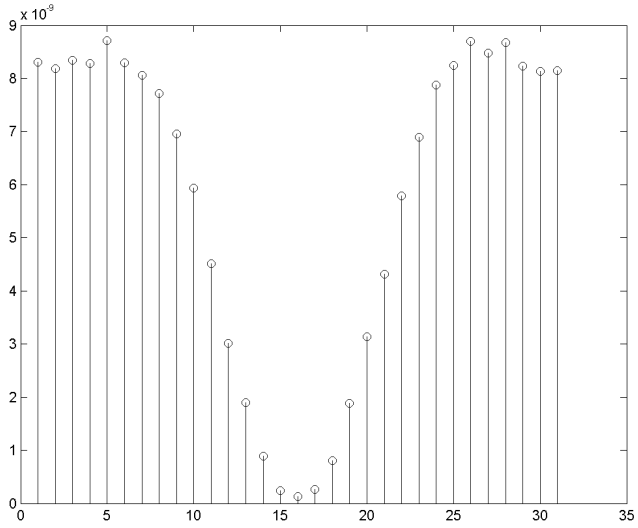

Figure 5c. The $D.O.S$ vector for the pipeline after the measurement array has been shifted by three units to the right. This is now presented as the test vector to the PNN for classification.

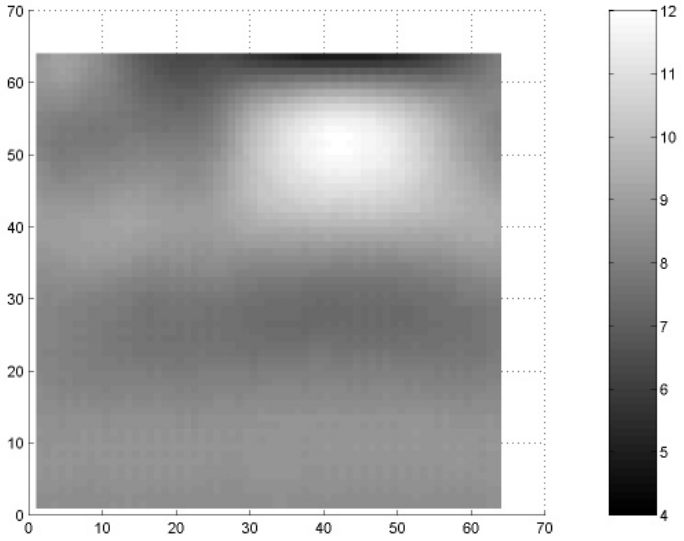

Figure 6a. The reconstructed permittivity considering the entire investigation domain.

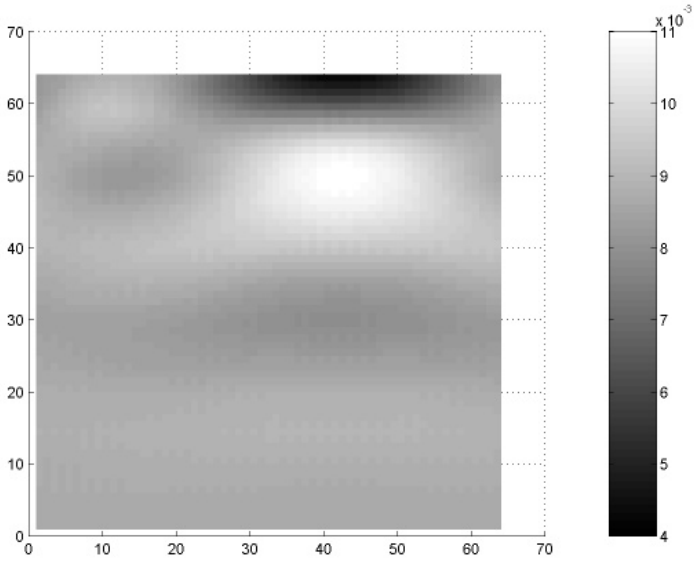

Figure 6b. The reconstructed conductivity considering the entire investigation domain.

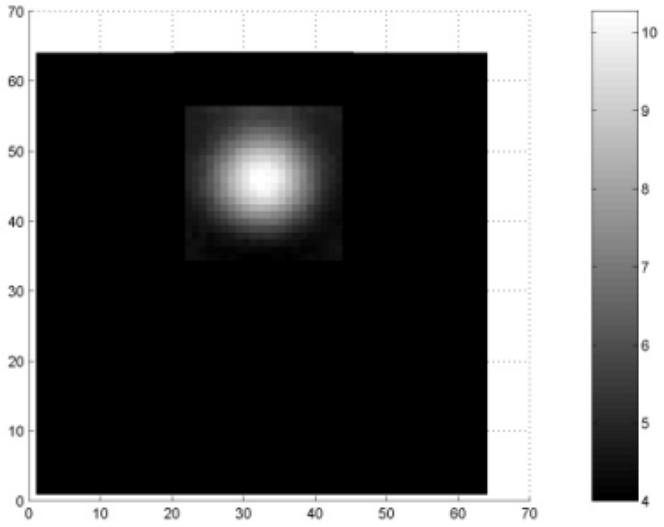

Figure 7a. The reconstructed permittivity with a reduced investigation domain. The coordinate system has been shifted so that the center of the pipeline cross section lies on the y-axis.

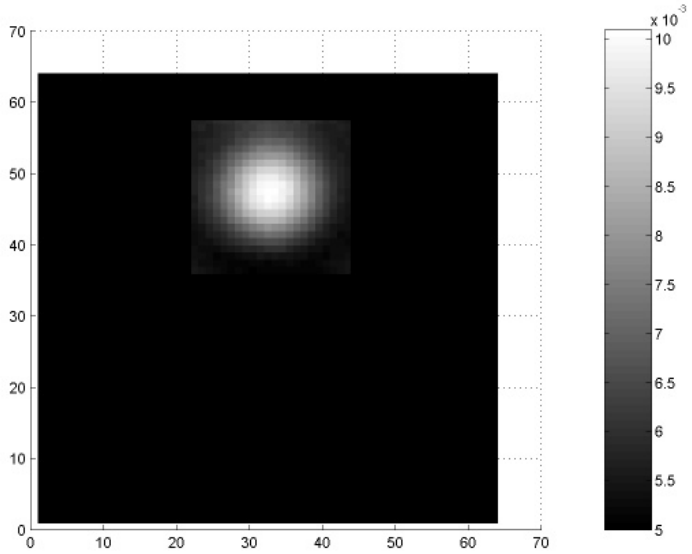

Figure 7b. The reconstructed conductivity with a reduced investigation domain. The coordinate system has been shifted so that the center of the pipeline cross section lies on the y-axis.

classifies it into one of the target classes that indicate the location of the centre of the scatterer and its radius. The reconstructed permittivity and conductivity images, after the 4th DBIM iteration considering the entire imaging domain are shown in Figure 6. When the $D.O.S$ vector is employed for the localization of the cylindrical scatterer, the PNN classifier classifies the scatterer as belonging to a reduced localized region of 22×22 pixels. Thus the strategy is found to be tolerant to noise. This is attributed to the robustness of the Probabilistic Neural Network in the presence of noise. Also, since the degrees of freedom in the inversion procedure are reduced by localizing the investigation domain, the robustness of the inversion procedure is improved.

The reconstructed profiles after the 4th DBIM iteration are shown in Figure 7. It is to be noted that the images obtained with the reduced investigation domain are always centered about the y-axis, as the centre of the pipeline is now aligned with the central transmitter. The reconstructed images are found to be much better when the localized imaging domain is employed than when the entire imaging domain is employed, in addition to reducing the computation time.

4. CONCLUSION

A novel preconditioning strategy for localizing the investigation domain in electromagnetic inverse profiling of buried 2-D dielectric pipelines with circular cross section has been presented. The entire measured scattered field data is available for the optimization of much fewer elements in the investigation domain. Thus there is a large data redundancy from which better reconstructions are obtained. The proposed technique reduces the degrees of freedom of the inverse scattering problem. The results are found to be far superior to those obtained when the entire imaging domain is employed.

ACKNOWLEDGMENT

Author Vinu Thomas thanks the Institute of Human Resource Development, Govt. of Kerala for providing sponsorship for the research. Author Jaimon Yohannan acknowledges CSIR, Human Resource Group, Ministry of HRD, New Delhi, India, for awarding Research Associateship. Authors Anil Lonappan and G.Bindu acknowledge CSIR, Human Resource Group, Ministry of HRD, New Delhi, India for awarding Senior Research Fellowship. Author K. T. Mathew thanks the Department of Science and Technology, Government of India, for the project SP/SO/D-22/98.

REFERENCES

1. Chew, W. C., *Waves and Fields in Inhomogeneous Media*, IEEE Press, New York, 1995.
2. Witten, A. J., J. E. Molyneux, and J. E. Nyquist, "Ground penetrating radar tomography: Algorithm and case studies," *IEEE Trans. Geosci. Remote Sensing*, Vol. 32, 461–467, 1994.
3. Deming, R. and A. J. Devaney, "Diffraction tomography for multi-monostatic ground penetrating radar imaging," *Inv. Problems*, Vol. 13, 29–45, 1997.
4. Souriau, L., B. Duchene, D. Lesselier, and R. Kleinman, "Modified gradient approach to inverse scattering of binary objects in stratified media," *Inv. Problems*, Vol. 12, 463–481, 1996.
5. Lambert, M., D. Lesselier, and B. J. Kooij, "The retrieval of a buried cylindrical obstacle by a constrained modified gradient method in the H-polarization case and for Maxwellian materials," *Inv. Problems*, Vol. 14, 1265–1283, 1998.
6. Chaturvedi, P. and R. G. Plumb, "Electromagnetic imaging of underground targets using constrained optimization," *IEEE Trans. Geosci. Remote Sensing*, Vol. 33, 551–561, May 1995.
7. Cui, T. J., W. C. Chew, A. A. Aydiner, and S. Chen, "Inverse scattering of two dimensional dielectric objects buried in lossy earth using the distorted Born iterative method," *IEEE Trans. Geosci. Remote Sensing*, Vol. 39, 339–345, Feb. 2001.
8. Cui, T. J., Y. Qin, G. L. Wang, and W. C. Chew, "Low-frequency detection of two dimensional buried objects using high order extended Born approximations," *Inv. Problems*, Vol. 20, S41–S62, 2004.
9. Thomas, V., C. Gopakumar, A. V. Praveen Kumar, V. Hamsakutty, A. Lonappan, G. Bindu, and K. T. Mathew, "A novel technique for reducing the imaging domain in microwave imaging of two dimensional circularly symmetric scatterers," *Microwave and Optical Technology Letters*, Vol. 44, No. 5, 423–427, March 2005.
10. Caorsi, S. and P. Gamba, "Electromagnetic detection of dielectric cylinders by a neural network approach," *IEEE Trans. Geosci. Remote Sensing*, Vol. 37, 820–827, March 1999.
11. Bermani, E., S. Caorsi, and M. Rafetto, "A microwave object recognition approach based on neural networks," *IEEE Instrumentation and Measurement Technology Conference Proceedings*, 1582–1585, Venice, May 1999.
12. Wasserman, P. D., *Advanced Methods in Neural Computing*, Van

Nostrand Reinhold, New York, 1993.

13. Harrington, F. R., *Field Computation by Moment Methods*, Macmillan, New York, 1968.
14. Duchene, B. and W. Tabbara, "Characterization of a buried cylindrical object from its scattered field," *IEEE Trans. Sonics Ultrasonics*, Vol. 31 658–663, 1984.
15. Specht, D. F., "Probabilistic neural networks for classification, mapping or associative memory," *Proceedings of the IEEE International Conference on Neural Networks*, Vol. 1, 525–532, IEEE Press, New York, 1988.